Robustness of a full-scale precast building structure subjected to corner-column failure

Manuel Buitrago [a], Nirvan Makoond [a,*], Juan J. Moragues [a], Juan Sagaseta [b], Jose M. Adam [a]

[a] *ICITECH, Universitat Politècnica de València, Camino de Vera s/n, 46022 Valencia, Spain*
[b] *School of Sustainability, Civil and Environmental Engineering, University of Surrey, GU2 7XH Guildford, UK*

ARTICLE INFO

ABSTRACT

Although many analytical and experimental studies have been carried out to date on the progressive collapse and robustness of cast-in-place reinforced concrete (RC) and steel building structures, very few experimental research works have been performed on precast concrete (PC) structures. The small number of publications on these experiments have focused on analysing the behaviour of subassemblies after the sudden loss of an internal column. This paper is the first to describe the construction of a full-scale purpose-built experimental PC building to study the sudden removal of corner columns and the structure's ability to find alternative load paths (ALPs). The connections between the precast members were designed using existing simplified guidance for robustness. The results obtained from the test using gravity loads corresponding to typical load combinations defined in building codes for accidental design situations, showed a structural response governed by Vierendeel action with a clear contribution from the floor slabs. Load increase factors were obtained from the test results which can be applied by practitioners using simplified linear finite element models to account for non-linear dynamic effects in a simplified manner. This work is expected to form part of a large database of experimental results that are useful for developing advanced numerical simulations and parametric analyses.

1. Introduction

Precast concrete construction has several advantages over cast-in-place buildings in terms of speed of construction, reduction of waste (i.e. more effective reuse of formwork), improved quality control and safety during construction. Special attention should be given to the connections between the elements, especially in case of accidents or extreme events, to ensure sufficient structural integrity to avoid a domino effect that could lead to total collapse of the building. Although good design practices and recommendations already exist for precast concrete elements [1], these can only safeguard against some of the known risks considered in design codes, e.g. seismic and wind loads.

Advanced codes and guides [2–6] introduce the concept of structural robustness or the capacity of the structure to adapt to and withstand local failure scenarios, regardless of the cause (threat-independent approach) and avoiding its propagation leading to progressive collapse. Structural robustness design can follow various methods to prevent progressive collapse, including indirect methods, e.g. tying approach, the alternative load path (ALP) method or the specific load resistance method [5]. The first consists of giving the structure enough continuity

through connections and/or ties to improve its structural response after local failures; the second consists of ensuring that the structure can find ALPs after the failure of any vertical load-bearing element, e.g. columns and walls in all parts of the structure; while the third consists of looking for key elements that would lead to progressive collapse if they fail, and to design them so as to reduce the possibility of failure to a minimum. The ALP method has attracted the most attention from researchers, who typically employ it to analyse a structure's capacity to generate ALPs after the sudden removal of any column (notional member removal approach) [7].

Fewer studies have been published on precast concrete structures than on cast-in-place reinforced concrete (RC) structures with respect to the notional member removal approach [7]. Apart from numerical and analytical studies, experimental studies in the field of precast RC structures have focused on testing subassemblies formed by two beams and three columns in which the middle column is removed [8–27]. Only one test was performed on 2-bay frames with two floors [28] to analyse their capacity to find other ALPs that had never been tested experimentally until then. In all these studies, it was found that the structural design of the joints affected the capacity of the structure to avoid the

---

Fig. 1. General overview and dimensions of the building-specimen.

propagation of a local failure of an internal or edge column. There are no available experiments looking at the influence of 3D effects of a structure and the contribution of the slabs for the case of corner columns. The influence of slabs redistributing the load is relevant for understanding the development of ALPs such as the Vierendeel action.

The novelty of the present study lies in the construction, testing and analysis of a complete full-scale building with precast RC elements. Testing corner columns in a complete building provides unique test data about ALPs compared to subassembly tests. The structure was extensively monitored during the test, which was carried out at an outdoor laboratory with the same conditions as an indoor laboratory with respect to characterization of the materials, the sensors used and the process control. The joints between the precast elements followed widely accepted structural design guidance [1,5,6] used in the sector, with special attention given to their effect on the robustness of the structure. It is also significant to remark that corner columns are more vulnerable and exposed to extreme events compared to other columns [29,30].

The overall aim of the study was to determine ALPs after the sudden loss of a corner column, when the building is subjected to gravity loads with values given in design codes for accidental load combinations. Another objective of this work was to determine the Load Increase Factors (LIFs) which are generally used in current practice; LIF are applied to static loads in linear numerical models to take into account non-linear and dynamic effects in a simplified manner.

After this Introduction, the paper contains a description of the test building in Section 2. Section 3 describes the monitoring system, while

Section 4 includes the results and analyses of the test. The discussion, which includes the ALP analyses and the calculation of the LIFs, is included in Section 5, while Section 6 gives the main conclusions drawn from the work.

2. Description of the building and test

The purpose-built structure had two 2.6 m-high floors measuring 15 × 12 m² in plan, with three 5 m bays in one direction and two 6 m bays in the other (Fig. 1). The building was designed in accordance with Eurocodes [31–33] with 2.5 kN/m² dead load and 5.0 kN/m² live load (appropriate for use categories C3, C4, C5, D1 and D2 according to Eurocode 1 [32]), and following the recommendations of the Institution of Structural Engineers (IStructE) [6] and the FIB [1,5] for the connections and tying systems for robustness.

The foundations were cast in place with sleeves to later connect with the concrete columns by grouting (Fig. 2). The 40 × 40 cm² columns were precast and the beams were partially precast and had total dimensions of 40 × 60 cm² (width × depth; the precast part was 40 × 35 cm², with a cast-in-place topping of around 25 cm). During construction, these beams were simply supported with elastomeric supports on the column corbels (width and length: 40 cm; depth: 30 cm along the variable length plus 30 cm along the constant length), which had two 20 mm diameter dowel bars for their connection. The final beam-column connection was arranged using top continuity reinforcement through 3 ties that crossed the internal columns through the tubular sleeves

Fig. 2. Details of the building during construction: foundation (a), connections prepared for ties in edge, internal and corner columns (b) and placing of hollow-core units for the slabs (c).

(Fig. 2b) and reached the corner columns where the ties were threaded and anchored to the columns (Fig. 2b). 3×20 mm diameter (942 mm^2) tie bars were used in peripherical beams, while 3×25 mm diameter (1473 mm^2) tie bars were used in internal beams (from C5 to C8 only). The cross-sectional area of ties in the beams was similar to that recommended by the DoD [4] (935 mm^2 and 1869 mm^2 for peripherical and internal ties, respectively), with considerably more reinforcement than that recommended by the Eurocode [2] (218 mm^2 and 435 mm^2 for peripherical and internal ties, respectively) but less than that recommended by the FIB [5] (1114 mm^2 and 2227 mm^2 for peripherical and internal ties, respectively, with a limitation of vertical displacement of 1.1 m, the maximum rotation recommended by the DoD). The effective area of tying reinforcements in the building was larger than the values given above due to the slab topping reinforcement (described below). After installing the tie bars, the mortar grouting was injected in column sleeves and beam sleeves for the reinforcement and dowel bars. 20 cm-thick hollow-core slabs, oriented in the direction of the longest span of the building, were simply supported (using elastomeric supports) on

beams during construction until placing of the topping (Fig. 2c). 12 mm-diameter ties between hollow-core units themselves and between hollow-core units and beams were provided (Fig. 3a) following IStructE recommendations [6]. Continuity between bays was also ensured by 503 mm^2/m reinforcement bars along the top of the internal beams and connecting with the hollow-core slabs (Fig. 3a). All the structural elements were connected in this way to prevent collapse propagation during an accidental event. After placing a reinforcement layer on the top of the hollow-core units, a concrete topping 6.5 cm thick was placed, together with that of the top part of beams (Fig. 3b). Table 1 gives the reinforcement in the precast elements and in the cast-in-place part of the slabs.

The test took place 33 days after placing the concrete topping. The mechanical properties of the materials of the different elements were determined and mean values obtained on the day of the test are shown in Table 2.

The test involved the sudden removal of the C12 corner column, which was achieved by means of a specially designed unidirectional

Fig. 3. Details of the slab ties and continuity bars (a) and concrete topping on the slabs (b).

Table 1
Summary of the steel reinforcement.

Element	ID	Floor/Slab	Steel reinforcement
Columns	C1, C4, C9	Ground	8Φ16
Columns	C2, C10, C11	Ground	8Φ20
Columns	C8	Ground	4Φ20 (corners) + 4Φ16
Columns	C6, C7	Ground	8Φ25
Columns	C1, C4, C5, C8, C9, C12	1st floor	8Φ12
Columns	C2, C3, C6, C7, C10, C11	1st floor	8Φ16
Corbels	Support of perimetral beams	Ground – 1st floors	6Φ10 (long.) + 2Φ8 (stirrups)
	Support of internal beams	Ground – 1st floors	7Φ12 (long.) + 3Φ8 (stirrups)
Beams (precast)	Perimetral (Long direction) and internal	1st − 2nd slabs	Bottom: 5Φ16
			Top: 5Φ12
Beams (precast)	Perimetral (Short direction)	1st − 2nd slabs	Bottom: 5Φ16
			Top: 5Φ10
Precast hollow-core slab units	P20-2	1st − 2nd slabs	According to the supplier [34]
Slabs (topping)	—	1st − 2nd slabs	One rebar Φ8 each 20 cm

triple-hinged steel column (Fig. 4) allowing free movement of the column in the diagonal direction (C12-C7), thus also allowing it to move vertically. For the removal, the central hinge was unlocked by removing different locking systems and a slight destabilization of the column was imposed using a forklift. A similar system had previously been used by the authors [29,30]. A gravity load was introduced in the structure with a value corresponding to the quasi-permanent combination of actions for accidental design situations given in the Eurocode [31] (1.0xDL + 0.3xLL; where DL are Dead Loads and LL are Live Loads). This loading consisted of a uniformly distributed load of 4 kN/m² composed of concrete blocks, applied only in the corner bay of both the first and second floors. Fig. 4 contains views of the steel column to be removed and of the concrete blocks.

3. Monitoring

During the column-removal test, data was acquired at a sample rate of 200 Hz from a total of 106 sensors, including 59 strain gauges, 38 displacement transducers and 9 accelerometers.

As detailed in Table 3, two strain gauges were placed on either side of the collapsible steel column (Fig. 5c) to monitor the change in axial strains due to unloading during the sudden column-removal. The remaining 57 strain gauges were embedded in the concrete and placed either on longitudinal rebars in columns (Fig. 5), on the continuous ties placed in beams, on ties between hollow-core units, on continuity bars and u-shaped ties, on the reinforcement mesh bars in the topping, or on dowel bars.

The locations of all the strain gauges placed on the continuity reinforcement of the beams and slabs are shown in Fig. 6, while the locations

Table 2
Mechanical properties of the concrete and steel reinforcement of different elements.

Mechanical property	Element	Results
Compressive Strength [MPa]	Columns C2, C6, C7, C8, C10, C11	32.4
3 concrete cylinders per element;	Columns C1, C3, C4, C5, C8, C9, C12	34.2
300x150mm (EN 12390–3)	1st slab beams	41.8
	2nd slab beams	36.7
	Topping	34.1
Elastic Modulus [MPa]	Columns C2, C6, C7, C8, C10, C11	34,504
3 concrete cylinders per element;	Columns C1, C3, C4, C5, C8, C9, C12	30,000
300x150mm (EN 12390–13)	1st slab beams	35,645
	2nd slab beams	37,584
	Topping	33,527
Tensile Strength [MPa]	Columns C2, C6, C7, C8, C10, C11	2.40
3 concrete cylinders per element;	Columns C1, C3, C4, C5, C8, C9, C12	3.12
300x150mm (EN 12390–6)	1st slab beams	3.27
	2nd slab beams	2.82
	Topping	2.94
Reinforcement Yield Strength [MPa] *(EN ISO 15630-1)*	Φ12 (4 specimens)	590
	Φ25 (4 specimens)	532
Reinforcement Tensile Strength [MPa] *(EN ISO 15630-1)*	Φ12 (4 specimens)	717
	Φ25 (4 specimens)	656
Reinforcement Elongation after Fracture *(EN ISO 15630-1)*	Φ12 (4 specimens)	21.5%
	Φ25 (4 specimens)	23.4%
Reinforcement Elongation at Maximum Force *(EN ISO 15630-1)*	Φ12 (4 specimens)	8.6%
	Φ25 (4 specimens)	14.4%

Load on the 1st slab

Load on the 2nd slab

Hinges

Fig. 4. Steel column designed for the sudden removal and load superimposed on the 1st and 2nd slabs.

Table 3
Summary of strain gauge locations.

Strain gauge locations	No. of strain gauges
Collapsible steel column	2
Longitudinal rebars in columns	32
Continuous ties in beams	13
Ties between hollow-core units	2
Continuity bars and u-shape ties between hollow-core slabs and beams	5
Reinforcement mesh in topping	3
Dowel bars between corbels and beams	2
Total	**59**

of those placed in columns are shown in Fig. 7. It should be noted that the strain gauges on the bars of the reinforcement mesh in the topping and on dowel bars are not shown in Fig. 6. Of the three strain gauges placed on the reinforcement mesh, two were on the first floor and one on the second floor, in close vicinity to column C12. With respect to the two strain gauges placed on the dowel bars, one was on a corbel in column C12 and the other on the opposite corbel in column C11 on the side with three 5 m-span bays.

Of the 38 displacement transducers used, 20 were for monitoring vertical displacements while 18 were for monitoring horizontal displacements. As summarised in Table 4, vertical displacement transducers were used either to monitor differential foundation settlements (Fig. 8a) or placed on spring-loaded telescopic bars to monitor the change in the vertical distance between the ground and the first floor

Fig. 5. (a) Strain gauge placed on column reinforcement before applying protective covering putty; (b) Strain gauge placed on column reinforcement prior to concreting; (c) strain gauge placed on collapsible steel column.
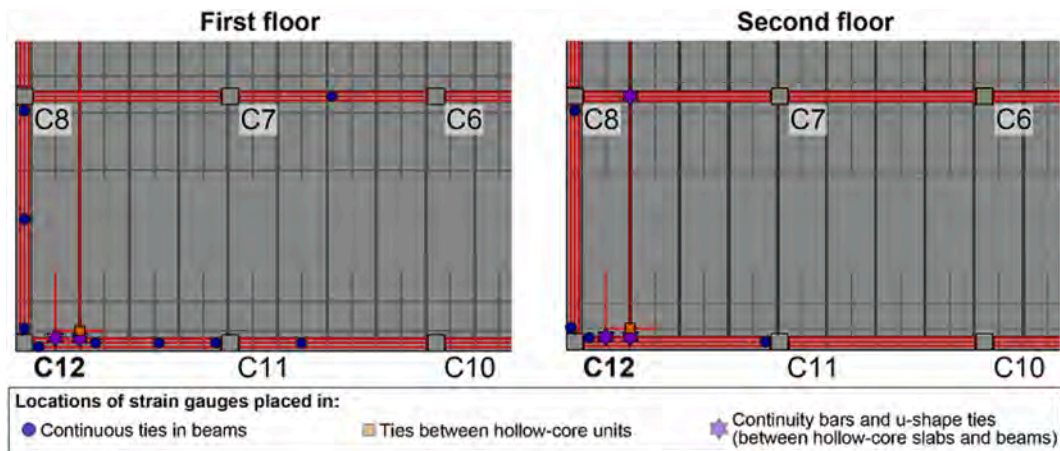

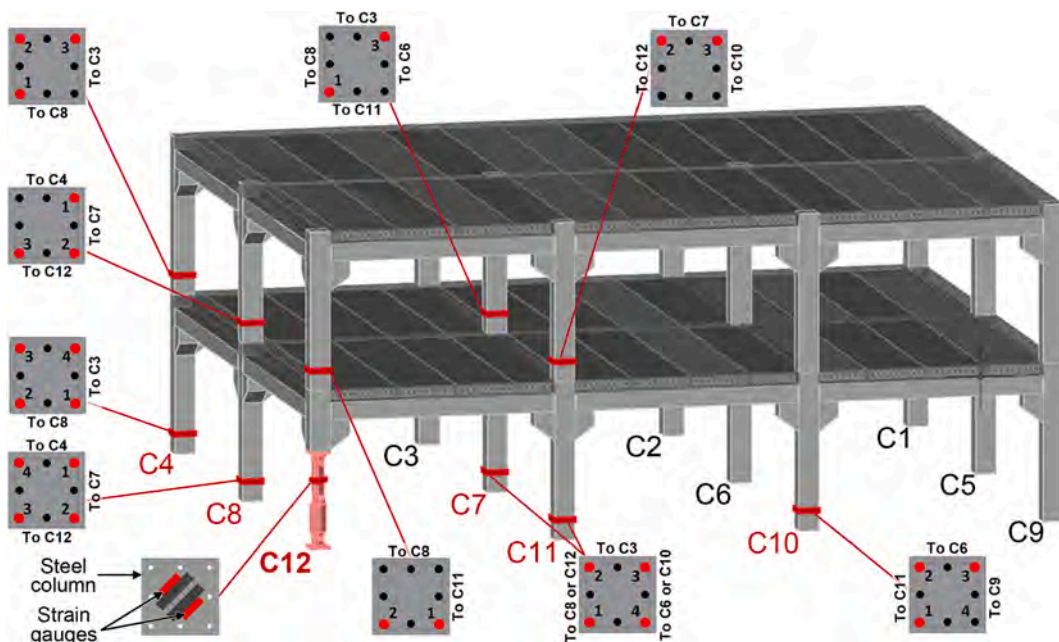**Fig. 6.** Locations of strain gauges placed over main reinforcements for continuity in beams and slabs.

Fig. 7. Locations of all strain gauges placed in columns.

Table 4
Summary of displacement transducer locations.

Displacement transducer locations	No. of sensors
Vertical displacement	
Foundation settlement	3
Between ground floor and first floor	9
Between first floor and second floor	8
Horizontal displacement	
Building drift	4
Top of beam-column joint	7
Bottom of beam-column joint	5
Joint between hollow-core units	2
Total	**59**

Fig. 8. Displacement transducer used to monitor: (a) vertical settlement of foundation, (b) vertical displacement of first floor, (c) building drift (connected to detached auxiliary structure), and (d) horizontal contraction at the bottom of beam-column joint.
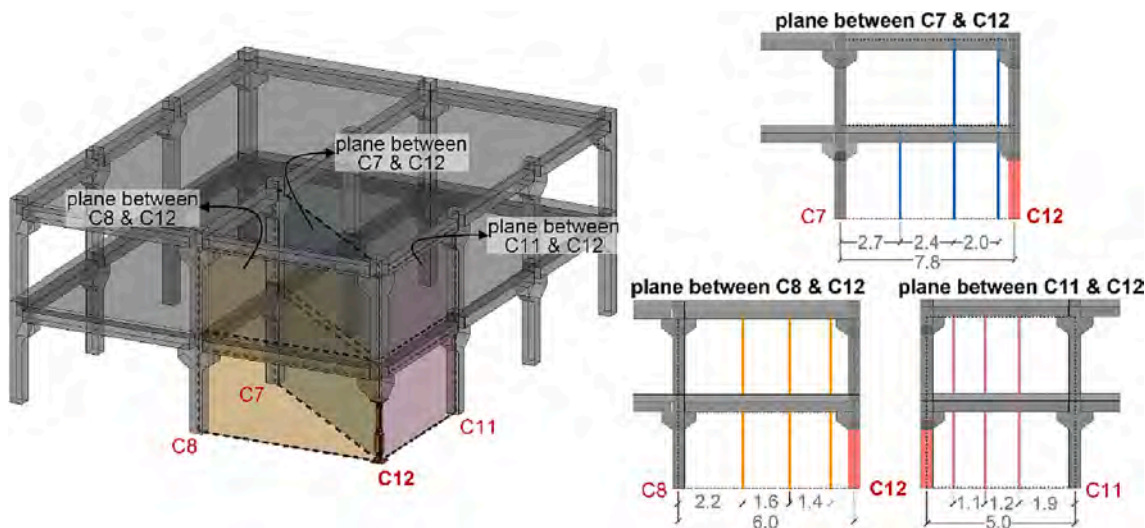
Fig. 9. Locations of all displacement transducers used to measure relative vertical displacement between floors (all dimensions shown in m).

(Fig. 8b) or between the first and second floors. The horizontal transducers were used to monitor building drift (Fig. 8c) or the horizontal expansion and contraction on the top or bottom of beam-column joints (Fig. 8d) or between the hollow-core precast units.

The exact locations of all the displacement transducers used to measure the relative vertical displacement between floors are shown in Fig. 9. The three transducers used to monitor foundation settlements were placed above the C7, C8 and C11 column foundations. The positions of the horizontal displacement transducers are shown in Fig. 10.

The accelerometers used for the test were fibre-optic uniaxial sensors. Of the 9 sensors, 6 were based on Fibre Bragg Grating (FBG) technology and used for monitoring the dynamic response of the structure after the sudden column removal. The remaining 3 were more sensitive Fabry-Pérot (FP) accelerometers. These were used prior to column removal for ambient vibration tests of (i) the undamaged structure, (ii) the structure after the column removal, and (iii) the damaged structure after returning the collapsible steel column to its original position. The positions of the accelerometers and their measurement directions are shown in Fig. 11.
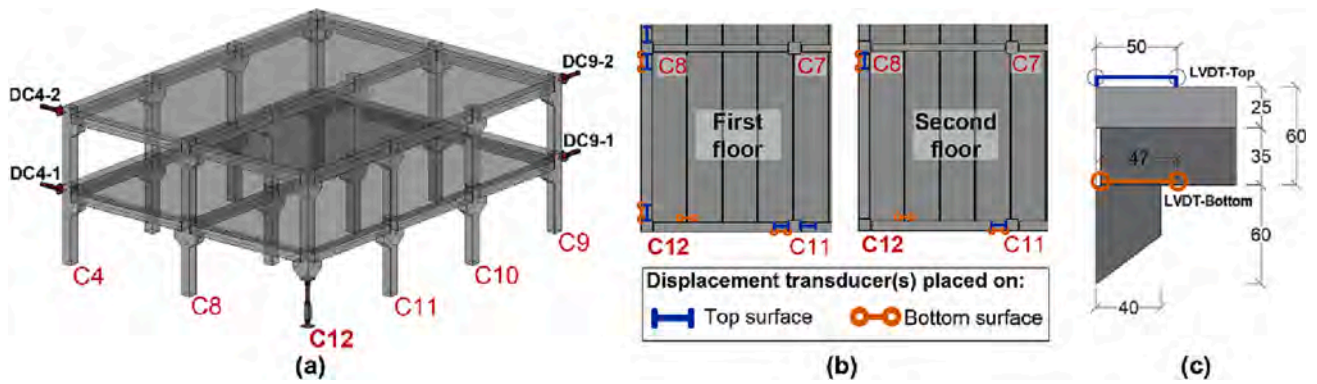
Fig. 10. (a) Locations of displacement transducers monitoring horizontal building drift; (b) Displacement transducers monitoring horizontal extension or contraction at the top or bottom of beam-column joints or below the slab between hollow-core planks; (c) Schematic showing the positioning of displacement transducers at the top and bottom of a beam-column joint (all dimensions shown in cm).
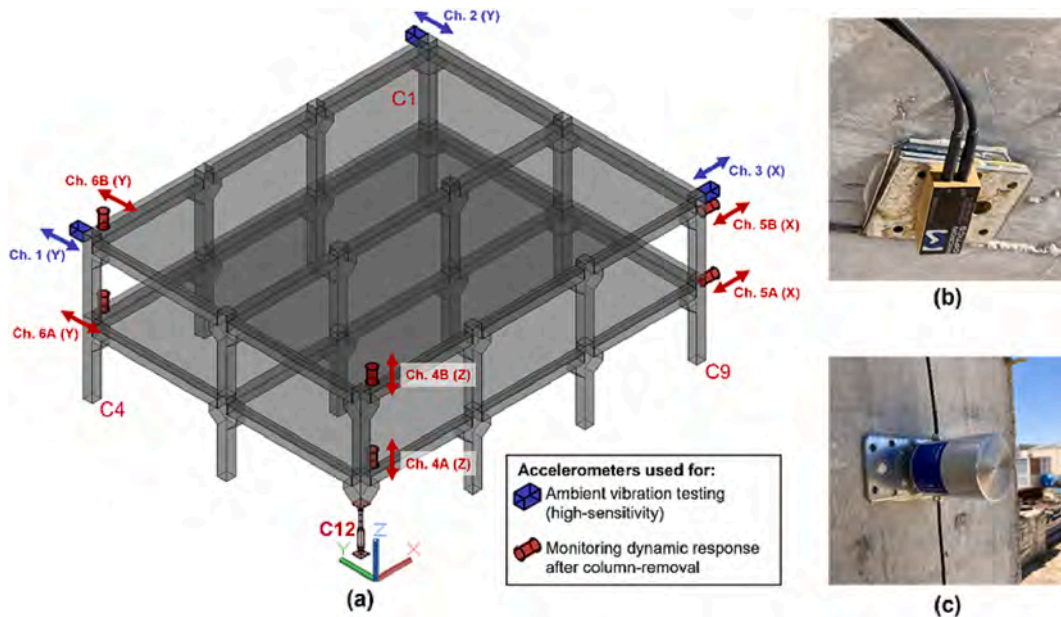

Fig. 11. (a) Locations and direction of measurement of all accelerometers used; (b) High-sensitivity accelerometer used for ambient vibration testing; (c) Accelerometer used for monitoring dynamic response after column removal.

4. Results and analyses

Test results are presented and analysed in this section, which is organised according to the following subsections: strain readings, vertical and horizontal measurements, accelerations and the state of the structure after the test.

4.1. Strain readings

Strain readings were taken from reinforcement bars in different elements such as columns, ties, slabs and dowels only during the test from an initial value of zero.

Fig. 12 gives the results obtained from column C12 in the sudden
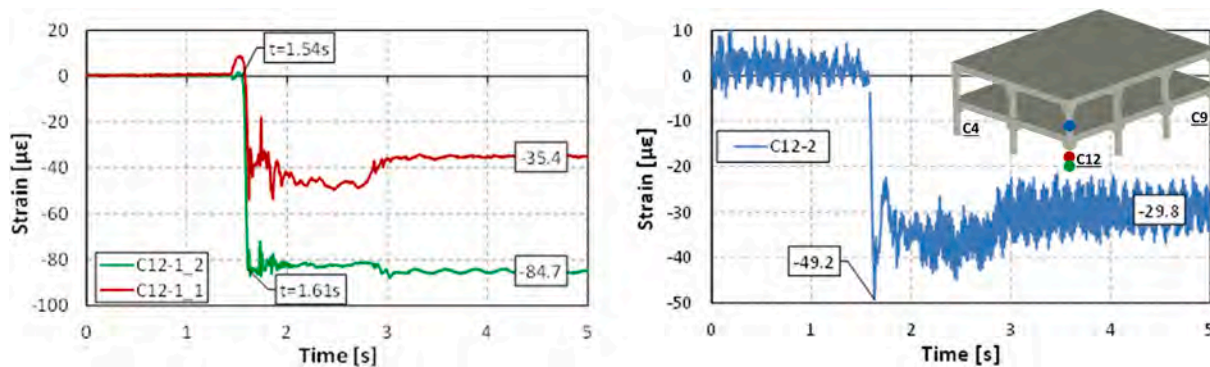
Fig. 12. Strain readings on the first-floor steel C12 column (left) and average strain reading on the second-floor concrete C12 column (right). Positive values indicate compression.

corner-column removal on the ground floor. The readings from the first-floor gauges show that the total unloading time was 0.07 s. The results from the second-floor show that column C12 unloaded (49.2 με at peak value and 29.8 με at the residual value), causing the column to change from an axial compression state (106 kN) to an axial tension state (130 kN at peak and 37 kN at residual value). In no case did the tension reach the concrete cracking strength and always remained below 0.82 MPa.

Fig. 13 gives the results of Columns C7, C8, C11 (Fig. 13a-c), C4 and C10 (Fig. 13). Fig. 13a-b,d gives the average reading of the different strain gauges as a representative measure of the axial strain readings of the column, whereas Fig. 13c shows all the strain readings of column C7. Column C7 did not experience a rise in its mean deformation (see Fig. 13a), although there were significant variations in individual deformation values (see Fig. 13c), which indicate the rotation of this column towards the removed column C12. In columns C8 and C11, a similar response can be seen, both on the first (Fig. 13a) and second floors (Fig. 13b). In both cases, the columns suffered higher compression. In columns C4 and C10, however, slight axial decompression can be seen, confirming the rocking effect of the outer frames.

Table 5 contains all the peak and residual values of the strain gauges installed on columns, together with a scheme of the sensors in each column (plan view). The strain values obtained could be used to determine the axial and bending moments using a nonlinear sectional approach with moment–curvature diagrams for different axial forces.

Fig. 14 shows the strain results from the peripheral ties on beams both close to columns and at mid-span between columns. It can be seen that (i) the strains were well below the plastic deformation (over 2500 με) and (ii) the positions close to the nodes present very high tensile deformations (shown in green in Fig. 14a-d) which are much lower than at mid-span. These results suggest that the ties were not activated by catenary action but by large bending moments due to Vierendeel action. This was confirmed by the compression values measured in the strain gauges in the ties close to the removed column C12 (shown in red in Fig. 14a-b). The values were generally higher in the C12-C11 beam than in the C12-C8 beam, due to the former being shorter (5 m) than the latter (6 m).

Fig. 15 shows the results from the reinforcement mesh of the concrete topping, the reinforcement in the interconnection between precast units in the transverse direction, the continuity bars between precast units (longitudinal directions), and U-shape ties between precast units and beams. The results from the reinforcement mesh (Fig. 15a) show compression values, again demonstrating positive bending moments in the zone near the removed column C12 due to Vierendeel action. These compressions in the slab topping also show the important contribution of the slabs to redistributing loads and searching for ALPs after the column removal. Similar conclusions can be drawn regarding the ties
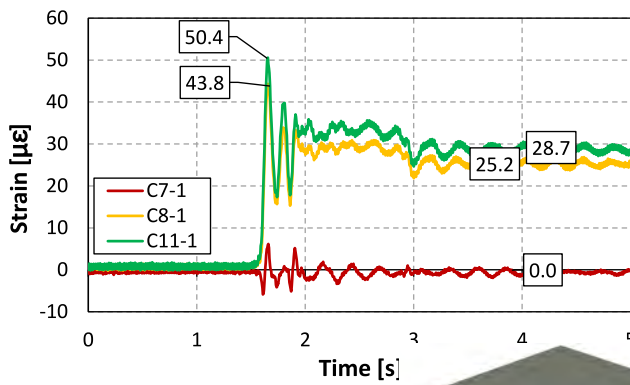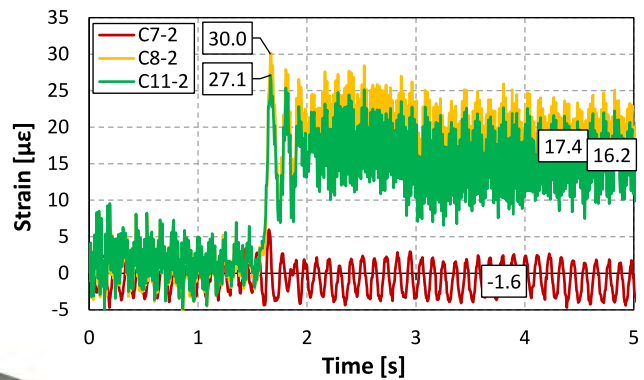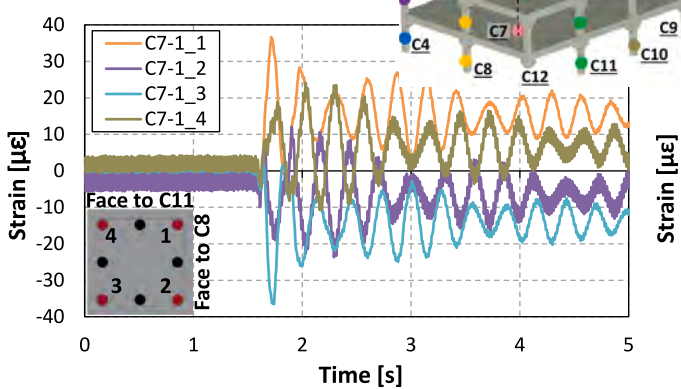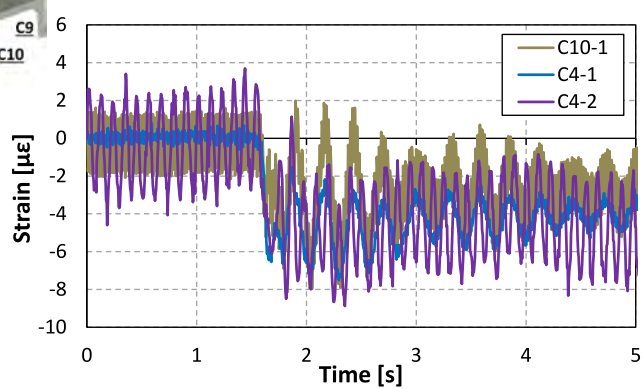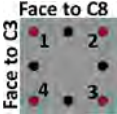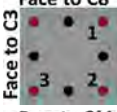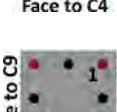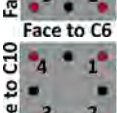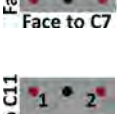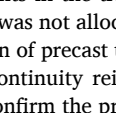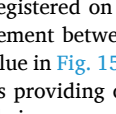

Fig. 13. (a-b) Average strain readings of the columns closest (Columns C7, C8 and C11) to the removed column; (c) strain readings of all sensors of columns C7, and (d) average strain readings of columns C4 and C10. Positive values indicate compression.

Table 5

Peak and residual strain readings of sensors placed on concrete columns. Positive values indicate compression.

Column	Floor	Sketch	Sensor	Peak [με]	Residual [με]
C4	1		C4-1_1	28.8	8.2
			C4-1_2	−22.4	−5.7
			C4-1_3	−38.6	−17.9
			C4-1_4	−15.1	−1.5
C4	2		C4-2_1	27.2	9.8
			C4-2_2	−13.1	−7.7
			C4-2_3	−30.4	−17.7
C7	1		C7-1_1	36.6	14.2
			C7-1_2	−23.7	−7.6
			C7-1_3	−36.4	−14.0
			C7-1_4	24.2	6.7
C7	2		C7-2_1	16.8	5.6
			C7-2_2	—	—
			C7-2_3	14.6	9.2
C8	1		C8-1_1	33.0	8.2
			C8-1_2	62.3	41.6
			C8-1_3	61.2	41.0
			C8-1_4	28.9	8.2
C8	2		C8-2_1	20.8	12.5
			C8-2_2	39.0	27.7
			C8-2_3	31.5	15.0
C10	1		C10-1_1	31.6	7.0
			C10-1_2	−19.5	−4.3
			C10-1_3	−28.9	−12.0
C11	1		C11-1_1	63.0	39.1
			C11-1_2	62.0	32.7
			C11-1_3	46.1	16.8
			C11-1_4	44.5	21.4
C11	2		C11-2_1	—	—
			C11-2_2	29.8	11.6
			C11-2_3	21.7	13.9
C12	2		C12-2_1	−23.6	−10.3
			C12-2_2	−82.5	−56.2
			C12-2_3	—	—

between precast units in the transverse direction (Fig. 15b), although this reinforcement was not allocated to the slab for this purpose, but to avoid the separation of precast units under tension. The positive values registered in the continuity reinforcement between precast units and beams (Fig. 15c) confirm the previous findings, showing that compressive strains were registered on these strain gauges. The results of the continuity reinforcement between precast units in the longitudinal direction (shown in blue in Fig. 15c) show that this reinforcement worked under tension loads providing continuity to the slab and avoiding the precast units from being separated from the framed structure.

Fig. 16 shows the strain readings for the dowel reinforcement at the corbels. Significant differences can be seen between the dowels located at column C12 and the dowels located at C11. The dowel located at column C12 worked under tension loads since the beam tended to pull out of the corbel, but this slip was restraint by the ties and the dowel at the corbel. The dowel in C11 worked under compression loads due to the increased beam vertical reaction on the corbel after the removal of C12. More details about the behaviour of the dowels can be found in Section 4.3.

4.2. Vertical displacement measurements

Fig. 17 shows the vertical displacement of the foundations closest to the removed column (C7 shown in green; C8 in yellow and C11 in red), which were used to correct the results obtained in the building in the case of significant displacement. The vertical displacement was almost negligible for C11 (0.14 mm) and practically zero for C7 and C8.

Fig. 18 shows the vertical displacement or deformed shape of the C7-C12 profile (Fig. 18a) and of peripheral beams C8-C12 (Fig. 18b) and C11-C12 (Fig. 18c) on the first slab, in which the maximum drop registered reached a peak value of 12.1 mm. The relative vertical displacements between the first and the second slabs were small along profiles C7-C12 and C8-C12 as shown in Fig. 19; the measurements were taken at the same distance from the columns as in the first slab. A detailed analysis of these results can be found in Section 5.1.

4.3. Horizontal displacement measurements

The drifts measured in the building at the corners of columns C4 and C9 towards the removed column C12 are shown in Fig. 20. Higher values were registered in C4 than C9 since the C4-C12 frame only had two bays and was more flexible than frame C9-C12, with three. The values of the horizontal displacements were small (<1 mm) at the top slab and negligible in the first slab.

Another set of LVDTs measuring horizontal displacements were employed to estimate bending moments and deformations in beams close to the columns shown in Fig. 21, which gives the results obtained in the first slab (Fig. 21a-b; lines from C12 to C4 and from C12 to C10) and second slab (Fig. 21c; lines from C12 to C8 and C12 to C11). These results show the activation of Vierendeel action, with negative bending moments (hogging moments) in all beam-to-column joints except in the one near the removed column C12, where positive bending moments (sagging moments) were found. In general, the LVDTs that registered shortening displacements according to the above-explained criteria show very small values. These bending moments in the joints show that the semi-rigid corbel connections used between beams and columns (only the tie reinforcement passed from the beams through the columns) were able to mobilise bending moments due to the contribution of: i) the dowels working under shear loads (Fig. 22a-b); and ii) the cast-in-place upper part of the beam working under local bending moments (Fig. 22b).

Fig. 23 shows the measurements of the separation between the precast units in the first (red) and second slabs (green). The values measured were quite small and were higher in the second slab (0.017 mm) than the first (0.006 mm). These values show negligible separations between the precast units close to the removed column C12 and confirm a Vierendeel action that generated tension forces in the lower part of the slabs in these zones.

4.4. Acceleration values

Fig. 24 shows the vertical acceleration values (in C12 first and second slabs) and horizontal (in C4 and C9 first and second slabs) registered by fibre-optic accelerometers during the tests. The vertical accelerations associated with the oscillations generated after the column removal reached values of around 0.7 g with a peak value of up to 1.8 g. These values show that removing the corner column generated a movement with accelerations close to the free-fall of the building. The peak acceleration of 1.8 g suggests the development of higher frequency modes
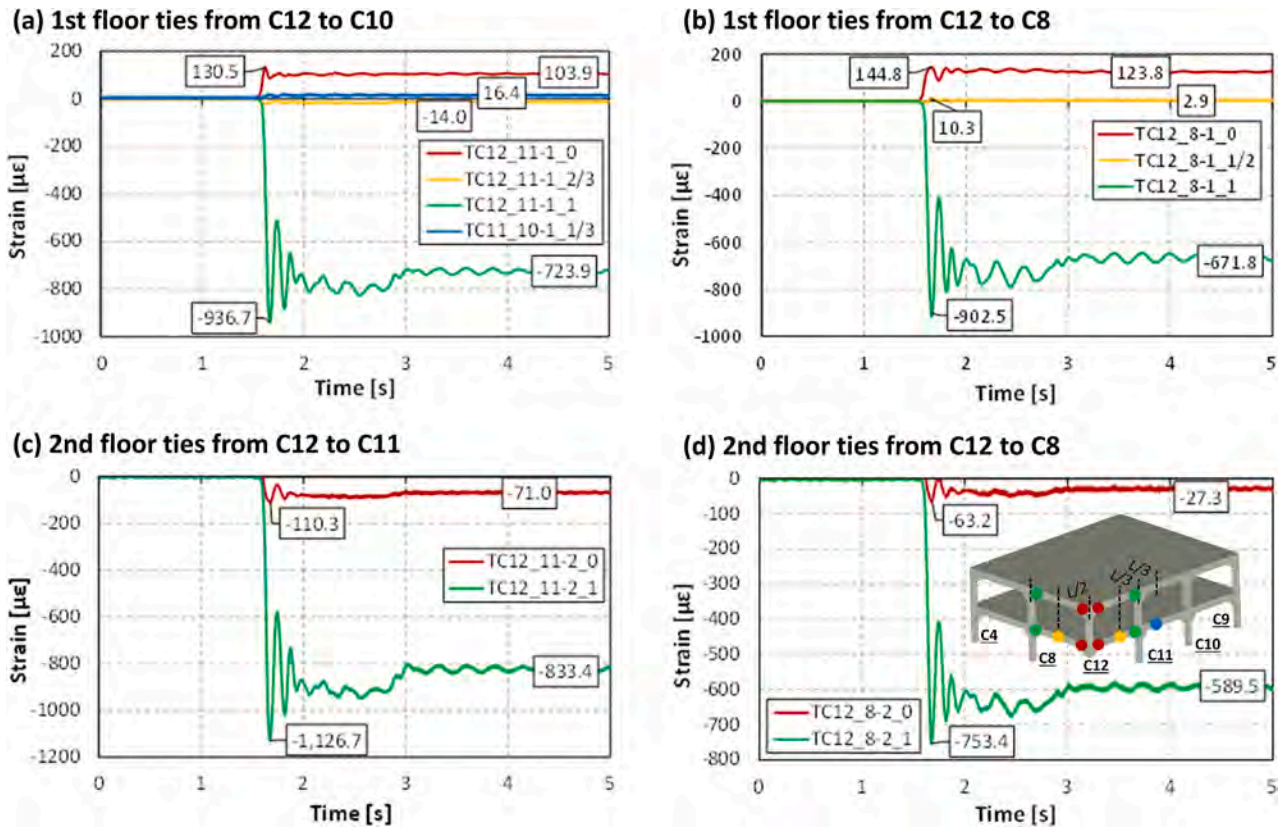
Fig. 14. Strain readings on first and second floor ties. Positive values indicate compression.
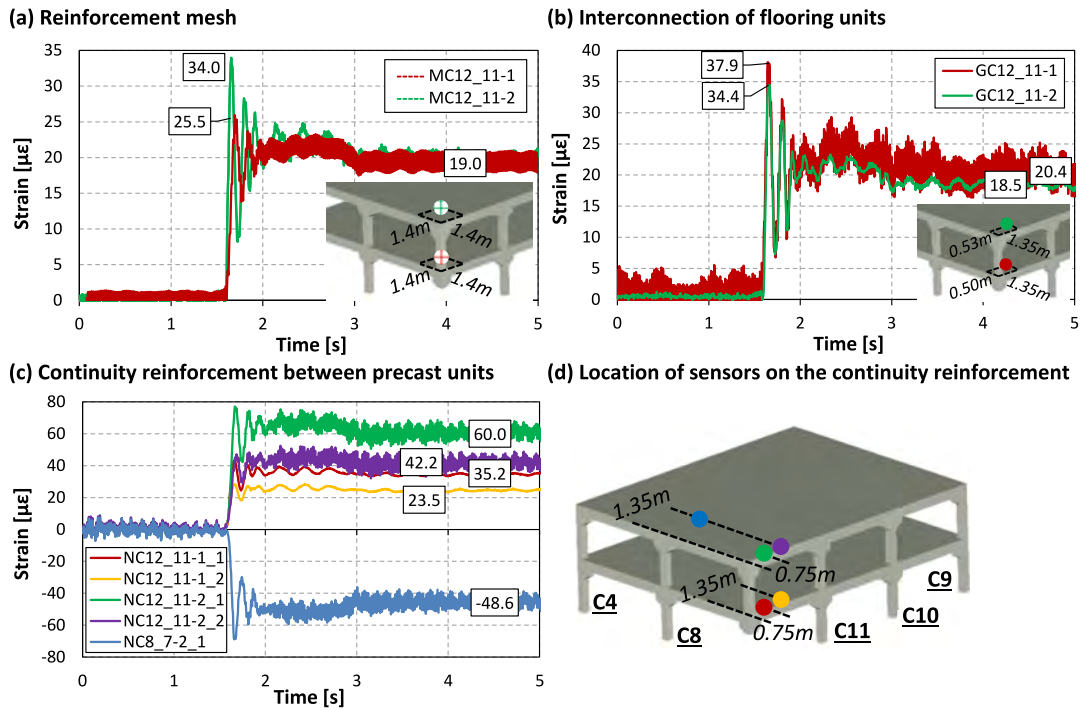

Fig. 15. Strain readings on (a) reinforcement mesh (M) and (b) interconnection of flooring units (G) of the first (red) and second (green) floors, and on (c-d) the continuity or tying reinforcement between precast units (N). Positive values indicate compression. (For interpretation of the references to colour in this figure legend, the reader is referred to the web version of this article.)
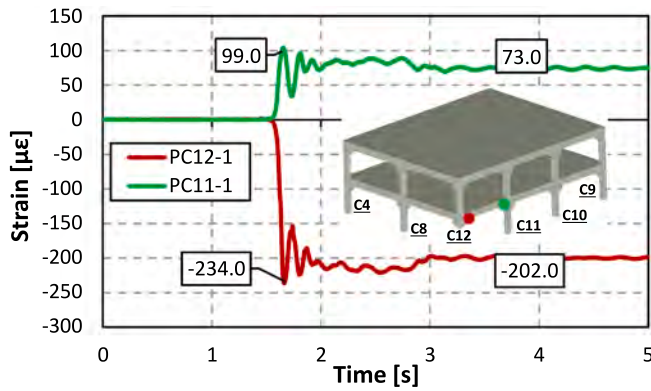
Fig. 16. Strain readings on dowels of Columns C12 and C11 (1st floor). Positive values indicate compression.

of vibration near the removed column due to the transmitted axial forces through the column above. A similar observation was made in a prior building test with infill masonry walls tested by the authors [30]. The horizontal accelerations were somewhat lower, with values during oscillations close to 0.4 g and up to 0.7 g.

4.5. Residual damage after the test

The structure only showed some minor residual damage after the column removal (cracking) around the beam-column connections. The state of the structure after the test can be seen in Fig. 25, which shows the state of the building with the hinged metal column (yellow box) that allowed the free fall of the corner (12.1 mm maximum drop). The cracks found after the test are also highlighted in the first slab beam-column joint C8 (red box) and C12 (green box). The first crack was due to hogging moments, as previously commented. The second crack was generated by the impact of the beam on the column due to localised compression in the beam where it touches the column.

5. Discussion

This discussion is divided into two parts, the first with an analysis of the ALPs activated in the structure after the sudden corner-column removal, and the second with the assessment of the Load Increase Factors (LIFs) [4] applied in simplified static linear numerical approaches to consider nonlinear and dynamic effects in a simplified manner.

5.1. Alternative load paths (ALPs)

The loads in the monitored columns during the test were also evaluated before the test, for which strains in the reinforcement were measured in the ground-floor columns C4, C7, C8, C10 and C11 at two different times, before building the structure (initial readings) and before the test. The loads estimated from strain measurements from the columns (Q_{real}) were compared with the results from a simplified FE model ($Q_{expected}$), see Section 5.2 for further details about this analysis. Table 6 compares the loads estimated from strain readings before the test with the predicted values from the FE model. According to the mean residual strain measurements in Table 3, the load increments on these columns after the tests were also quantified. Table 6 also gives the computed load increments and the final load on the columns obtained as the sum of the real initial loads and the load increments. As can be seen, all the monitored columns had a final compression load. The load on C12 before the sudden removal (estimated at 179.8 kN) was mainly redistributed through the outer frames and increased the load on C8 and C11 by 41% and 55%, respectively. There was also a rocking effect in the outer frames due to the unbalanced load after column removal in which the columns closest to the removed column (C8 and C11) had a total load increment of 288.5 kN, greater than the load suddenly removed from C12 (179.8 kN). This rocking effect resulted in the slight unloading of adjacent columns (e.g. C4 and C10) as shown in Table 6.

Besides the axial load redistribution of the columns after the removal of C12, as commented in Section 4, the structure activated Vierendeel action, as can be seen in Fig. 26a, with the peak and residual values of the deformed structural shape for alignments C11-C12 (shown in red),
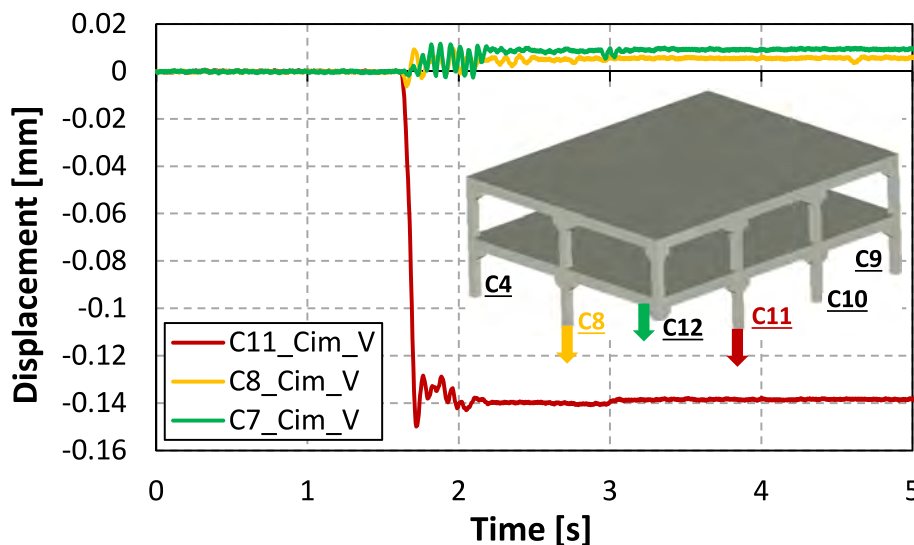

Fig. 17. Displacement measurements on foundations of columns C7, C8 and C11. Positive direction upwards.
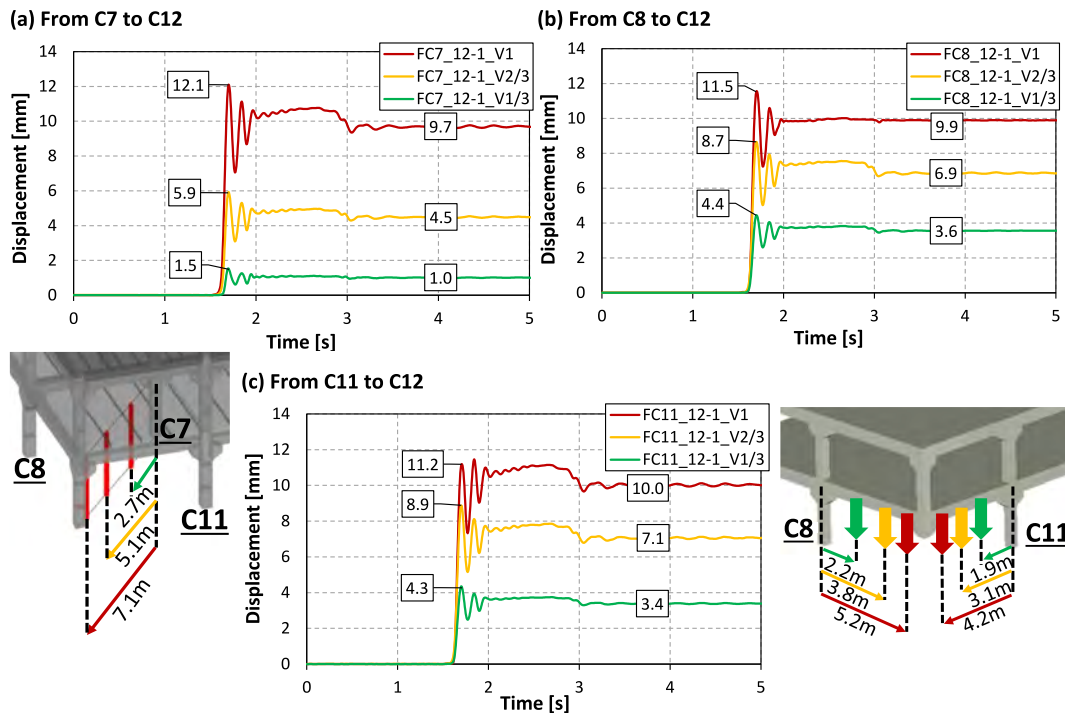
Fig. 18. Vertical displacement measurements on lines from columns C7, C8 and C11 to C12. First floor. Positive direction downwards.
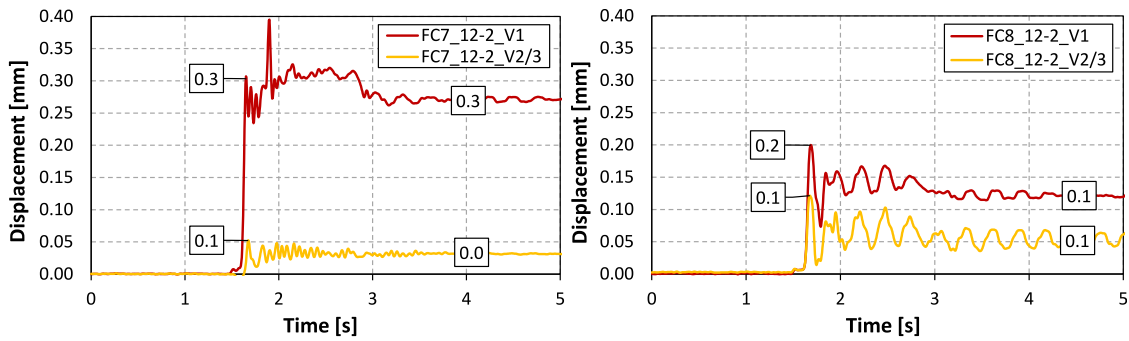

Fig. 19. Vertical displacement measurements on lines from columns C7 and C8 to C12. Second floor. Positive values indicate shortening.
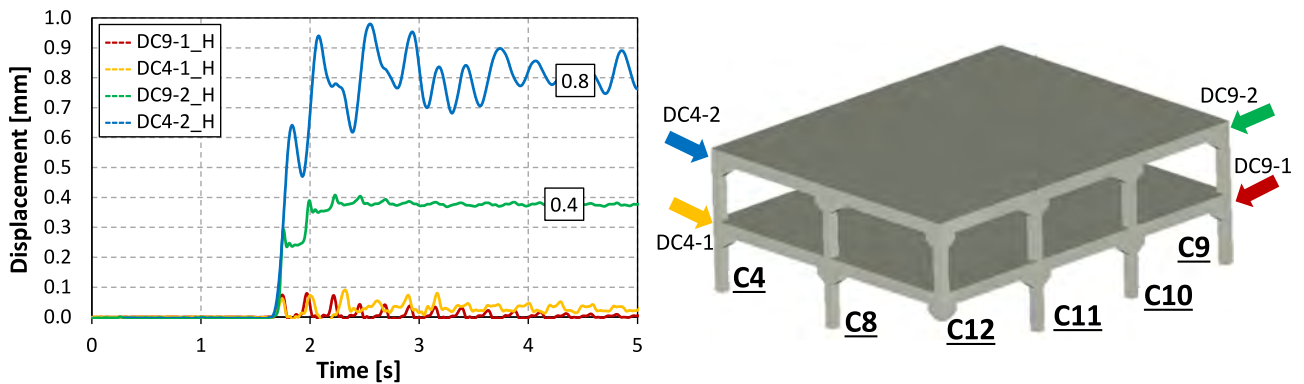

Fig. 20. Drifts measurements on the first and second floor columns C4 and C9. Positive values are indicated by arrows.
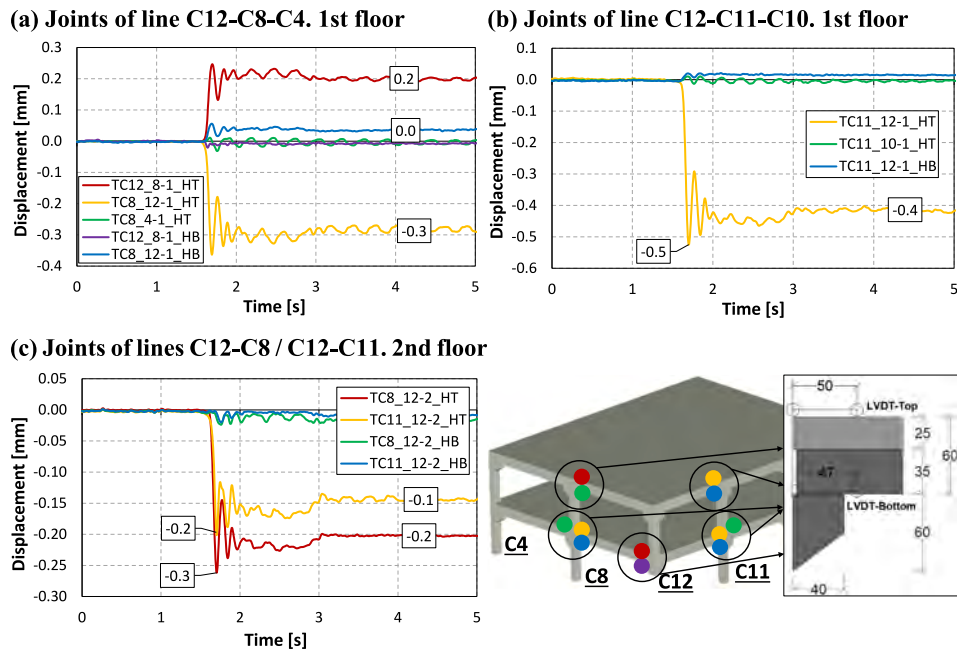
Fig. 21. Representative bending horizontal measurements of first (a-b) and second (c) floor beam-column joints. Shortening displacements are positive.
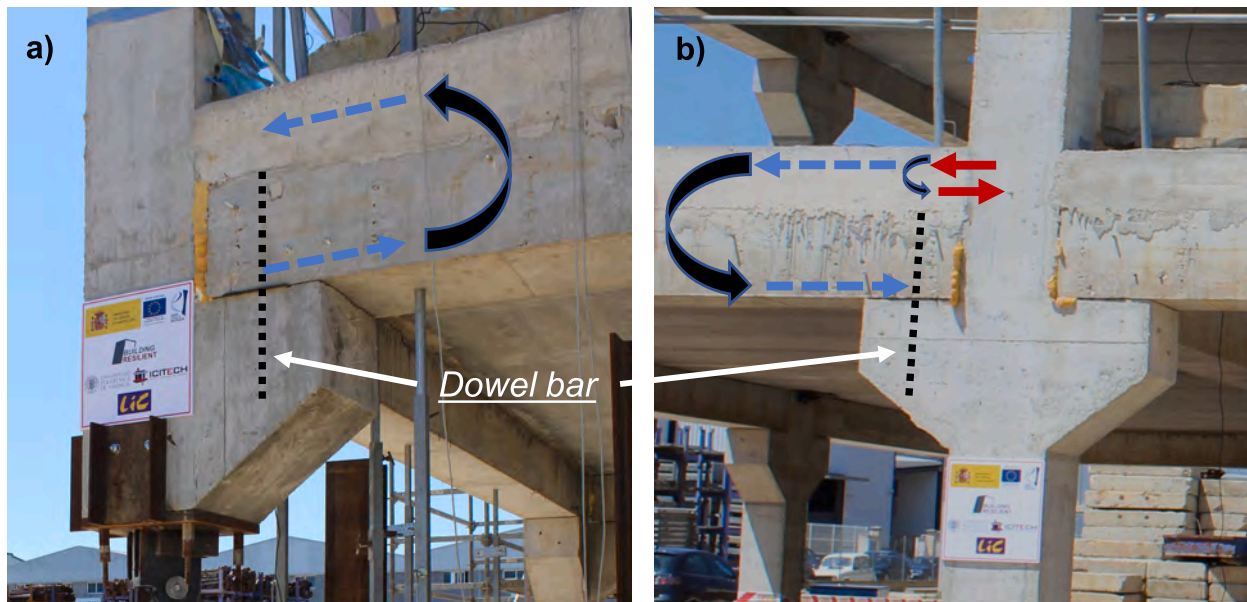

Fig. 22. Moment transfer on beam-column joints with the help of: dowel bars working under shear loads (a and b) and the cast-in-place upper part of the beam working under local bending moments (b only).

C8-C12 (in green) and C7-C12 (in blue). In the results of alignments C11-C12 and C8-C12 (edge frames) it can be seen that the deformed shape follows the pattern of a typical Vierendeel action due to flexure. However, along the C7-C12 diagonal the deformed shape follows more closely that of a cantilever since there was no system of frames to enable Vierendeel action, especially in the direction perpendicular to the precast units. It should be remembered that the hollow-core precast slab system only works in one direction and so has no capacity to activate

transversal positive bending moments.

Fig. 26b gives the horizontal displacements of C4 and C9, both of which tended to move towards the removed column C12. The C4-C8-C12 edge frame provided less lateral restraint against the column removal of C12 than the C9-C10-C11-C12 edge frame, which meant that the drift of the former after the test was twice as large as that of the latter.

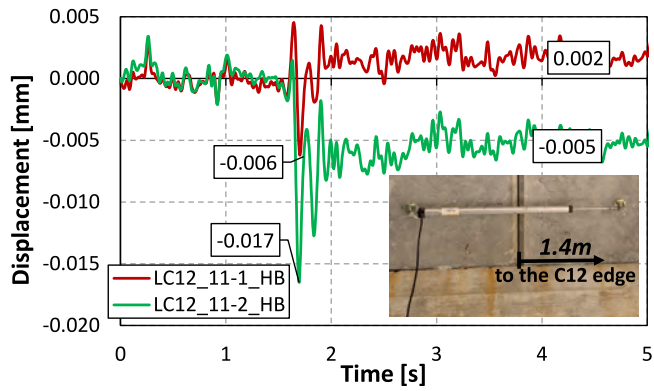Together with the results in Section 4, those given in this section

Fig. 23. Measurements of the separation between precast units on the first and second floors. Negative values indicate separation.

indicate that the main ALP activated after the sudden removal of C12 was Vierendeel action introducing: (i) bending on the beam-column joints and (ii) activating both directions in the entire 3D structure. It should be noted that Vierendeel action could be activated thanks to: i) the capacity of the semi-rigid beam-column joints to resist the bending moments due to the dowel and the cast-in-place upper part of the beam, and ii) the contribution of the slabs in redistributing the loads after the flexural deformations in the structure.

5.2. Assessment of load Increase Factors (LIFs)

Load Increase Factors (LIFs) or Dynamic Amplification Factors (DAFs) are frequently recommended in standards (e.g. DoD [4]) as a way of simplifying the analysis using numerical models after sudden column loss. This method can involve applying LIFs in computational models that do not consider non-linear material models or dynamic loads, while the DAFs can be applied as load factors in models that do not consider dynamic effects but do consider non-linear effects. This section describes a method of determining LIFs by a direct comparison of the dynamic and non-linear test results with those of a simplified FE model developed using the SAP2000 software [35] without considering neither material nonlinearities nor dynamic effects.

The FE model developed in this work reproduced the structure of the

Table 6
Initial and post-test reactions of the monitored columns.

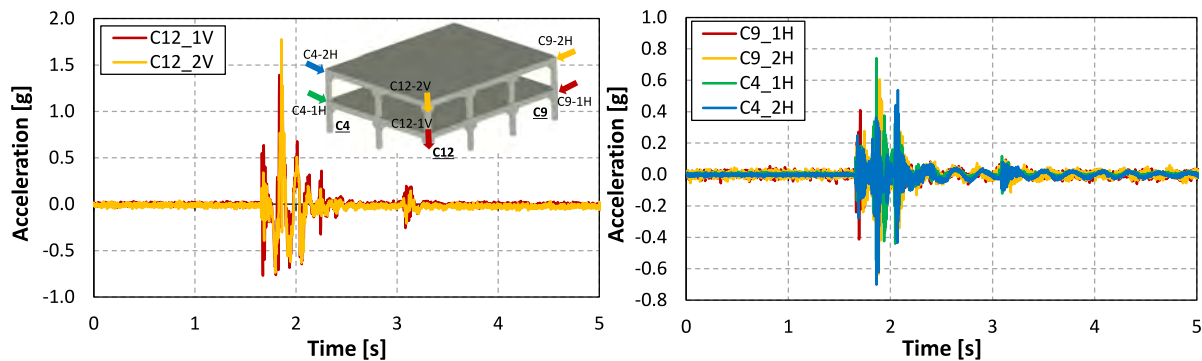| Columns	Initial loads			After test – Residual		
	Q_{real} [kN]	$Q_{expected}$ [kN]	Deviation [%]	Load increments [kN]	Final load [kN]	Increment [%]
C4	134.8	126.1	6.9%	−23.3	111.4	−17.3%
C7	481.9	476.3	1.2%	−1.0	481.0	−0.2%
C8	335.4	338.4	−0.9%	136.6	472.0	40.7%
C10	223.7	218.7	−2.3%	−17.1	206.6	−7.7%
C11	278.2	293.3	−5.2%	151.8	430.0	54.6%

Fig. 24. Vertical accelerations on the top of the removed column C12 and horizontal accelerations on the opposite corner columns C4 and C9.

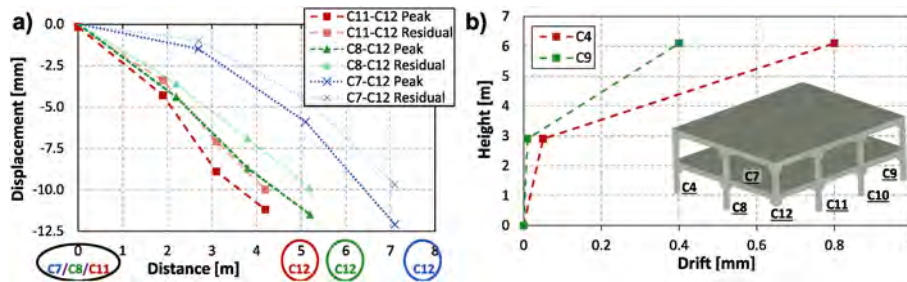**Fig. 25.** Structure after the test.

Fig. 26. Vertical deformed shape under first floor lines between C7-C12, C8-C2 and C11-C12; and drifts of columns C4 and C9.
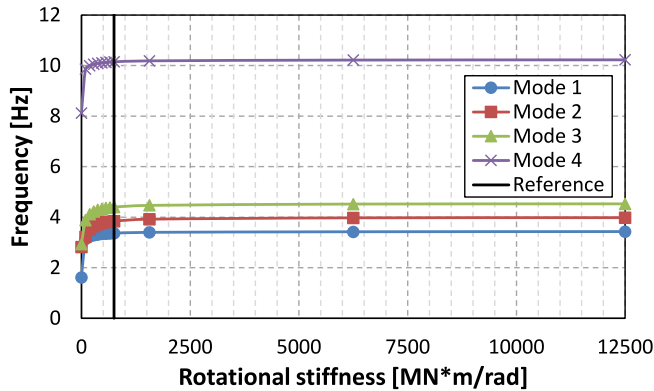

Fig. 27. Natural vibrational modes of the structure depending on rotational beam-column stiffness variation.

building used in the present study, including the values of the elasticity modulus for each of the elements, as described in Table 2. Columns, beams, and hollow-core precast units were modelled using beam elements, while the concrete topping in the slabs was modelled using shell elements. All the connections in the model were rigid to accurately represent the building, except those between beams and columns. The actual building had semi-rigid beam-column connections, represented by the tie reinforcement (acting as continuity reinforcement in the upper part of the beams), and the beams were also supported on the concrete corbels and connected by the dowel bars. These partially fixed connections can be represented by equivalent rotational springs. The real (unknown) exact situation can vary between simply supported (perfect hinge with zero rotational stiffness) and totally fixed connections. A rotational stiffness of 750 MN·m/rad was considered as representing a

totally connected beam-column joint (see Fig. 27). This value was adopted because the vibration modes of the FE model configured with such joints were in good agreement with those of an FE model with fixed connections. In addition, as shown in Fig. 27, further increasing the rotational stiffness causes no significant change in the vibration modes. Then it is understood that the stiffness of the structure does not vary because the beam-column joints have reached the condition of being rigidly connected (Mode 1: 3.37 Hz; Mode 2: 3.85 Hz; Mode 3: 4.41 Hz; Mode 4: 10.15 Hz). Fig. 28 shows the model developed in SAP2000, which was validated using the results presented in Section 5.1 (Table 6).

The LIFs were evaluated according to the rotational stiffness of the connections to study the influence of this parameter on the results. Different cases were investigated in the form of a parametric analysis from simply supported situations (0% as a perfect hinge) to totally fixed connections. Table 7 shows the LIF results for the forces (LIF$_{LF}$) and displacements (LIF$_{LD}$). Both of these factors were computed as the ratio of peak values obtained from the test (dynamic and nonlinear) and the corresponding values obtained from the FE analysis (static and linear). Axial loads in columns C8 and C11 were used to compute LIF$_{LF}$ while the maximum displacements (at the location of LVDT sensor FC7_12-1_V1) were used to compute LIF$_{LD}$. The simply-supported results (0%) were discarded since the displacements from the FE analysis were larger than the dynamic nonlinear displacements from the test. For the other cases, the computed LIF$_{LF}$ varied between 1.26 and 1.37, while the LIF$_{LD}$ varied between 1.07 and 2.47. The influence of connection stiffness was therefore significant for LIF$_{LD}$ and almost negligible for LIF$_{LF}$.

Refined LIF values were obtained using the rotational stiffness values for which the natural frequencies of the FE model best matched those obtained experimentally by means of Operational Modal Analysis (OMA) performed before the test (i.e. before structural damage). The experimental results (Mode 1: 3.82 Hz; Mode 2: 4.51 Hz; Mode 3: 5.11 Hz; Mode 4: 11.97 Hz) revealed that the best fit between the theoretical and experimental results could be obtained from the numerical model in
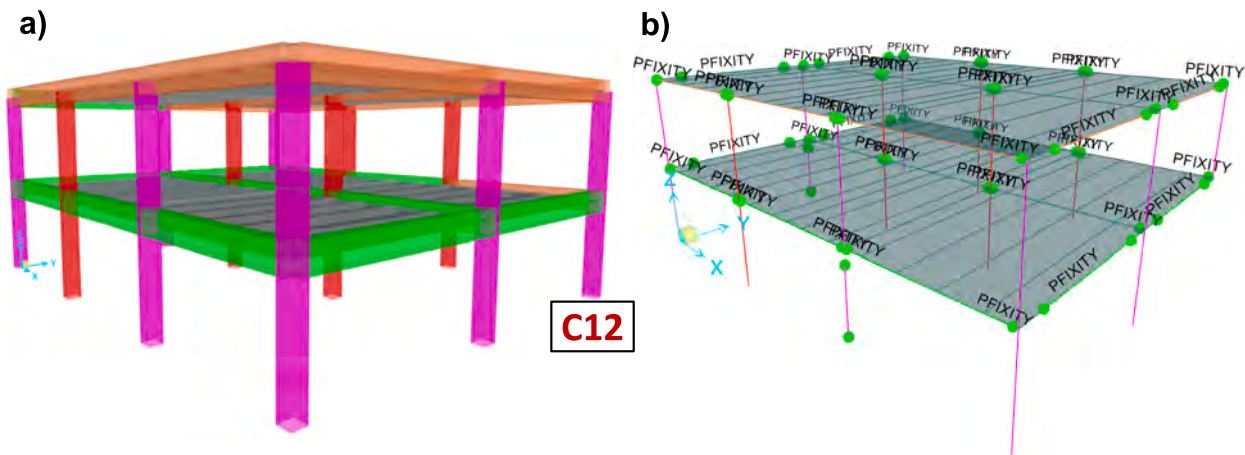

Fig. 28. FE model developed on SAP2000 with elements and material representation before column removal (a) and with the structural model with the springs after column removal (b).

Table 7
Load Increase Factors (LIFs) for forces and displacements.

Rotational stiffness [MNm/rad]	Column C8			Column C11			Displacement in FC7_12-1_V1 location		
	Static linear	Dynamic nonlinear	LIF_{LF}	Static linear	Dynamic nonlinear	LIF_{LF}	Static linear	Dynamic nonlinear	LIF_{LD}
	Q_{SAP} [kN]	Q_{real} [kN]		Q_{SAP} [kN]	Q_{real} [kN]		D_{SAP} [mm]	D_{real} [mm]	
0.0 (0.0%)	531.3	591.3	1.11	380.3	575.7	1.51	39.68	12.10	0.30
93.8 (12.5%)	468.6	591.3	1.26	421.5	575.7	1.37	11.30	12.10	1.07
187.5 (25.0%)	462.2	591.3	1.28	427.2	575.7	1.35	8.53	12.10	1.42
281.3 (37.5%)	459.1	591.3	1.29	429.4	575.7	1.34	7.40	12.10	1.64
375.0 (50.0%)	457.1	591.3	1.29	430.5	575.7	1.34	6.85	12.10	1.77
468.8 (62.5%)	456.8	591.3	1.29	431.2	575.7	1.34	6.48	12.10	1.87
562.5 (75.0%)	454.8	591.3	1.30	431.7	575.7	1.33	6.22	12.10	1.95
656.3 (87.5%)	454.1	591.3	1.30	432.0	575.7	1.33	6.03	12.10	2.01
750.0 (100.0%)	453.5	591.3	1.30	432.2	575.7	1.33	5.89	12.10	2.05
Connected	448.1	591.3	1.32	433.7	575.7	1.33	4.90	12.10	2.47

which the beam-column connections were totally fixed. This is a reasonable assumption, since the semi-rigid connections used in the structure can effectively be considered as being totally rigid under the effect of ambient vibrations and for loads which do not cause large displacements, as was the case in the test. According to this criterion, the recommended LIFs are 1.32 and 2.47, for forces and displacements respectively. While it is important to recall that LIFs depend on the magnitude of the total deformation as well as on section properties [36], it is interesting to note that the displacement-based LIF is greater than 2. This result is in good agreement with findings of previous studies for structural response in the inelastic range [37].

6. Conclusions and future work

The sudden removal of a corner column was tested for the first time in an experiment on a full-scale building made with precast concrete components. The experimental building was designed according to the latest international codes and standards in the field of progressive collapse and structural robustness. The structural details of the beam-column joints in the building were designed considering common building practices and the need to conserve structural integrity after the sudden removal of a corner column. After an exhaustive description of the building, the test, and the extensive monitoring carried out, the results obtained were analysed and the Alternative Load Paths (ALPs) activated by the structure were determined. The Load Increase Factors (LIFs) that can be used to increase the design load in simplified computational models were also obtained. These are typically employed to indirectly consider complex dynamic and nonlinear effects in assessments using linear elastic models. From the results obtained, it can be concluded that:

- Although the beam-column joints are semi-rigid with no apparent bending resistance, the main ALP was Vierendeel action, which demands flexural behaviour in these joints. This flexural behaviour was possible due to i) the dowel bars working under shear loads and the cast-in-place upper part of the beam working under tension; and ii) the cast-in-place upper part of the beam working under local bending moments. These two contributions to the bending capacity of the semirigid joint could not be easily expected and quantified before the test. This prevented the structure from mobilising its last lines of structural defence normally associated with catenary and membrane actions.
- The contribution of the slabs in the load redistribution after flexural deformations in Vierendeel action was significant, especially in its capacity to absorb bending moments in the principal direction of the hollow-core precast units.
- The load suddenly withdrawn from column C12 was mostly redistributed through the edge frames by increasing the load on nearby columns by more than 40%. A rocking effect was also produced in

these frames due to the unbalanced loads. This resulted in nearby columns experiencing a load increment larger than the load removed from C12 and other columns further from C12 experiencing a slight unloading effect.

Results presented in this work are expected to be used to create a database of experimental results that are useful for the development of advanced numerical simulations and parametric analyses.

Declaration of Competing Interest

The authors declare that they have no known competing financial interests or personal relationships that could have appeared to influence the work reported in this paper.

References

[1] FIB Commission 6. Guide to good practice: Structural connections for precast concrete buildings. Lausanne (Switzerland): 2008.
[2] European Committee for Standardization (CEN). EN 1991-1-7:2006: Eurocode 1 - Actions on structures - Part 1-7: General actions - accidental actions. 2006.
[3] GSA. Alternate path analysis & design guidelines for progressive collapse resistance. Washington, DC: General Services Administration; 2013.
[4] Department of Defense (DoD). UFC 4-023-03: Unified Facilities Criteria - Design of buildings to resist progressive collapse 2009.
[5] FIB Commission 6. Guide to good practice: Design of precast concrete structures against accidental actions. Lausanne (Switzerland): 2012.
[6] The Institution of Structural Engineers (IStructE). Practical guide to structural robustness and disproportionate collapse in buildings 2010.
[7] Adam JM, Parisi F, Sagaseta J, Lu X. Research and practice on progressive collapse and robustness of building structures in the 21st century. Eng Struct 2018;173: 122–49. https://doi.org/10.1016/j.engstruct.2018.06.082.
[8] Nimse RB, Joshi DD, Patel PV. Behavior of wet precast beam column connections under progressive collapse scenario: an experimental study. Int J Adv Struct Eng 2014;6:149–59. https://doi.org/10.1007/s40091-014-0072-3.

[9] Kang S-B, Tan KH, Yang E-H. Progressive collapse resistance of precast beam–column sub-assemblages with engineered cementitious composites. Eng Struct 2015;98:186–200. https://doi.org/10.1016/j.engstruct.2015.04.034.

[10] Qian K, Liang S-L, Feng D-C, Fu F, Wu G. Experimental and numerical investigation on progressive collapse resistance of post-tensioned precast concrete beam-column subassemblages. J Struct Eng 2020;146:4020170. https://doi.org/10.1061/(ASCE) ST.1943-541X.0002714.

[11] Kang SB, Tan KH. Behaviour of precast concrete beam-column sub-assemblages subject to column removal. Eng Struct 2015;93:85–96. https://doi.org/10.1016/j.engstruct.2015.03.027.

[12] Zhou Y, Hu X, Pei Y, Hwang H-J, Chen T, Yi W, et al. Dynamic load test on progressive collapse resistance of fully assembled precast concrete frame structures. Eng Struct 2020;214:110675. https://doi.org/10.1016/j.engstruct.2020.110675.

[13] Kang S-B, Tan KH. Robustness assessment of exterior precast concrete frames under column removal scenarios. J Struct Eng 2016;142:4016131. https://doi.org/10.1061/(ASCE)ST.1943-541X.0001616.

[14] Kang SBB, Tan KHH. Progressive collapse resistance of precast concrete frames with discontinuous reinforcement in the joint. J Struct Eng 2017;143:1–13. https://doi.org/10.1061/(ASCE) ST.1943-541X.0001828.

[15] Tohidi M, Baniotopoulos C. Effect of floor joint design on catenary actions of precast floor slab system. Eng Struct 2017;152:274–88. https://doi.org/10.1016/j.engstruct.2017.09.017.

[16] Elsanadedy HM, Almusallam TH, Al-Salloum YA, Abbas H. Investigation of precast RC beam-column assemblies under column-loss scenario. Constr Build Mater 2017; 142:552–71. https://doi.org/10.1016/j.conbuildmat.2017.03.120.

[17] Almusallam TH, Elsanadedy HM, Al-Salloum YA, Siddiqui NA, Iqbal RA. Experimental investigation on vulnerability of precast RC beam-column joints to progressive collapse. KSCE J Civ Eng 2018;22(10):3995–4010.

[18] Qian K, Li B. Performance of precast concrete substructures with dry connections to resist progressive collapse. J Perform Constr Facil 2018;32:1–14. https://doi.org/10.1061/(ASCE)CF.1943-5509.0001147.

[19] Stathas N, Bousias SN, Palios X, Strepelias E, Fardis MN. Tests and simple models of RC frame subassemblies for postulated loss of column. J Struct Eng 2018;144:1–14. https://doi.org/10.1061/(ASCE)ST.1943-541X.0001951.

[20] Al-Salloum YA, Alrubaidi MA, Elsanadedy HM, Almusallam TH, Iqbal RA. Strengthening of precast RC beam-column connections for progressive collapse mitigation using bolted steel plates. Eng Struct 2018;161:146–60. https://doi.org/10.1016/j.engstruct.2018.02.009.

[21] Quiel SE, Naito CJ, Fallon CT. A non-emulative moment connection for progressive collapse resistance in precast concrete building frames. Eng Struct 2019;179: 174–88. https://doi.org/10.1016/j.engstruct.2018.10.027.

[22] Lin K, Lu X, Li Y, Guan H. Experimental study of a novel multi-hazard resistant prefabricated concrete frame structure. Soil Dyn Earthq Eng 2019;119:390–407. https://doi.org/10.1016/J.SOILDYN.2018.04.011.

[23] Zhou Y, Chen T, Pei Y, Hwang H-J, Hu X, Yi W, et al. Static load test on progressive collapse resistance of fully assembled precast concrete frame structure. Eng Struct 2019;200:109719.

[24] Qian K, Liang S-L, Fu F, Fang Q. Progressive collapse resistance of precast concrete beam-column sub-assemblages with high-performance dry connections. Eng Struct 2019;198:1–16. https://doi.org/10.1016/j.engstruct.2019.109552.

[25] Qian K, Li B. Strengthening and retrofitting precast concrete buildings to mitigate progressive collapse using externally bonded GFRP strips. J Compos Constr 2019; 23:1–15. https://doi.org/10.1061/(ASCE)CC.1943-5614.0000943.

[26] Qian K, Liang S-L, Xiong X-Y, Fu F, Fang Q. Quasi-static and dynamic behavior of precast concrete frames with high performance dry connections subjected to loss of a penultimate column scenario. Eng Struct 2020;205:110115. https://doi.org/10.1016/J.ENGSTRUCT.2019.110115.

[27] Feng F-F, Hwang H-J, Yi W-J. Static and dynamic loading tests for precast concrete moment frames under progressive collapse. Eng Struct 2020;213:110612. https://doi.org/10.1016/J.ENGSTRUCT.2020.110612.

[28] Wang F, Yang J, Shah S. Effect of horizontal restraints on progressive collapse resistance of precast concrete beam-column framed substructures. KSCE J Civ Eng 2020;24:879–89. https://doi.org/10.1007/s12205-020-1035-9.

[29] Adam JM, Buitrago M, Bertolesi E, Sagaseta J, Moragues JJ. Dynamic performance of a real-scale reinforced concrete building test under a corner-column failure scenario. Eng Struct 2020;210:110414. https://doi.org/10.1016/j.engstruct.2020.110414.

[30] Buitrago M, Bertolesi E, Sagaseta J, Calderón PA, Adam JM. Robustness of RC building structures with infill masonry walls: tests on a purpose-built structure. Eng Struct 2021;226:111384. https://doi.org/10.1016/j.engstruct.2020.111384.

[31] European Committee for Standardization (CEN). EN 1990:2002: Eurocode 0 - Basis of structural design 2002.

[32] EN 1991-1-1. Eurocode 1: Actions on structures. Part 1-1: Densities, self-weight, imposed loads for buildings; 2003.

[33] European Committee for Standardization (CEN). EN1992-1-1:2004: Eurocode 2 - Design of concrete structures - Part 1-1 : General rules and rules for buildings 2004.

[34] Ribe Prefabricados de Hormigón SL. Precast hollow-core slab units 2022.

[35] Computers & Structures Inc. SAP2000 v24 Ultimate 2022.

[36] Marchand K, McKay A, Stevens DJ. Development and Application of Linear and Non-Linear Static Approaches in UFC 4-023-03. Struct. Congr. 2009, Reston, VA: American Society of Civil Engineers; 2009, p. 1–10. https://doi.org/10.1061/41031(341)191.

[37] Tsai M-H, You Z-K. Experimental evaluation of inelastic dynamic amplification factors for progressive collapse analysis under sudden support loss. Mech Res Commun 2012;40:56–62. https://doi.org/10.1016/j.mechrescom.2012.01.011.